

The Role of Structural Order in the Mechanism of Charge Transport across Tunnel Junctions with Various Iron-Storing Proteins


Nipun Kumar Gupta, Naofumi Okamoto, Senthil Kumar Karuppannan, Rupali Reddy Pasula, Zhang Ziyu, Dong-Chen Qi, Sierin Lim, Masakazu Nakamura,* and Christian A. Nijhuis*

In biomolecular electronics, the role of structural order in charge transport (CT) is poorly understood. It has been reported that the metal oxide cores of protein cages (e.g., iron oxide and ferrihydrite nanoparticles (NPs) present in ferritin and E2-LFtn, which is E2 protein engineered with an iron-binding sequence) play an important role in the mechanism of CT. At the same time, the NP core also plays a major role in the structural integrity of the proteins. This paper describes the role of structural order in CT across tunnel junctions by comparing three iron-storing proteins. They are (1) DNA binding protein from starved cells (Dps, diameter (\varnothing) = 9 nm); (2) engineered archaeal ferritin (AfFtn-AA, \varnothing = 12 nm); and (3) engineered E2 of pyruvate dehydrogenase enzyme complex (E2-LFtn, \varnothing = 25 nm). Both holo-Dps and apo-Dps proteins undergo CT by coherent tunneling because their globular architecture and relative structural stability provide a coherent conduction pathway. In contrast, apo-AfFtn-AA forms a disordered structure across which charges have to tunnel incoherently, but holo-AfFtn-AA retains its globular structure and supports coherent tunneling. The large E2-LFtn always forms disordered structures across which charges incoherently tunnel regardless of the presence of the NP core. These findings highlight the importance of structural order in the mechanism of CT across biomolecular tunnel junctions.

1. Introduction

Charge transport (CT) across proteins immobilized inside tunnel junctions can be remarkably efficient. However, it is still unclear what the underlying mechanisms of CT are or which requirements such biomolecular junctions have to fulfill to observe efficient CT.^[1–6] For instance, activation-less conduction of charges over up to tens of nanometers have been observed (so-called long-range tunneling) which cannot be readily explained by established models. For this reason, alternative models have been developed.^[4,5,7,8] The role of structural order, however, has not been explicitly addressed but, in general, proteins inside junctions are assumed to have ideal tertiary structure. The present work seeks to elucidate the role of structural order in CT across tunnel junctions. Three representatives of iron-storing molecules of globular shapes and cage-like structures are compared: (1) DNA binding protein from starved (nutrition) cells (Dps,

N. K. Gupta, S. K. Karuppannan, Z. Ziyu, C. A. Nijhuis
Department of Chemistry
National University of Singapore
3 Science Drive, Singapore 117543, Singapore
N. K. Gupta, C. A. Nijhuis
Centre for Advanced 2D Materials
National University of Singapore
6 Science Drive 2, Singapore 117546, Singapore

 The ORCID identification number(s) for the author(s) of this article can be found under <https://doi.org/10.1002/sml.202203338>.

© 2022 The Authors. Small published by Wiley-VCH GmbH. This is an open access article under the terms of the Creative Commons Attribution-NonCommercial License, which permits use, distribution and reproduction in any medium, provided the original work is properly cited and is not used for commercial purposes.

DOI: 10.1002/sml.202203338

N. Okamoto, M. Nakamura
Division of Materials Science
Nara Institute of Science and Technology
Ikoma, Nara 630-0192, Japan
E-mail: mnakamura@ms.naist.jp
S. K. Karuppannan
National Quantum Fabless Foundry (NQFF)
Institute of Materials Research and Engineering
2 Fusionopolis Way, Innovis Building, Singapore 138634, Singapore
R. R. Pasula, S. Lim
School of Chemistry, Chemical Engineering and Biotechnology
Nanyang Technological University
70 Nanyang Drive, Singapore 637457, Singapore
D.-C. Qi
Centre for Materials Science
School of Chemistry and Physics
Queensland University of Technology
Brisbane, Queensland 4001, Australia

diameter (\varnothing) = 9 nm),^[9] (2) engineered archaeal ferritin (AfFtn-AA, \varnothing = 12 nm),^[10] and (3) E2 protein engineered with iron-binding sequence (E2-LFtn, \varnothing = 25 nm).^[11] Dps is rigid while AfFtn-AA and E2-LFtn have a large conformational degree of freedom and, consequently, are expected to be prone to deformation upon immobilization inside junctions. These protein nanocages have an intrinsic iron storage feature which allows for the formation of iron oxides in the form of nanoparticles (NPs). We found that the mechanism of CT across junctions with Dps is always nearly independent of the temperature (T) (a signature of coherent tunneling, which is activationless in nature) regardless of whether the proteins had metal oxide cores, in contrast to those junctions with apo-AfFtn-AA and apo-E2-LFtn where CT is dominated by thermally activated CT (a signature of incoherent tunneling). All holo-protein junctions are dominated by activationless CT. This behavior can be explained as the apo-Dps retains its globular geometry whilst the other apo-proteins are not stable, and form disordered monolayers where charges have to hop between disordered protein fragments.

The mechanism of CT across biomolecular tunnel junctions can be divided into coherent and incoherent tunneling. The tunneling current density (J , in A cm⁻²) for coherent tunneling decays exponentially with the tunneling distance (d , in nm), and is described by the general tunneling equation

$$J = J_0 e^{-\beta d} \quad (1)$$

where β is the tunneling decay coefficient (in nm⁻¹) and J_0 is the pre-exponential factor. Coherent tunneling is activationless in nature. In contrast, incoherent tunneling is characterized by the Arrhenius equation involving over barrier hopping defined by the activation energy (E_a , in meV)

$$J = A e^{-\frac{E_a}{k_B T}} \quad (2)$$

where k_B is the Boltzmann constant and A is the pre-exponential factor. In principle, the observed J is a summation of incoherent and coherent processes, and the total tunneling current (J_{obs} , in A cm⁻²) can be summarized as

$$J_{\text{obs}} = J_0 \exp(-\beta d) + A \exp\left(-\frac{E_a}{k_B T}\right) \quad (3)$$

Beyond metal oxide cores (iron oxide NPs^[12,13] in this work), other cofactors (e.g., metal ion,^[14,15] small molecule^[16,17]) can

play a major role in the mechanism of CT. Junctions with various holo-proteins show activationless CT with high CT rates, but the CT mechanism of the same junctions lacking the metal oxide cores or cofactors changes to thermally activated CT with relatively low CT rates.^[10,15,16,18] For example, relatively large currents flow across junctions of various holo-proteins, including, halorhodopsin (with retinal and bacterioruberin cofactors),^[16] AfFtn-AA (with iron oxide NPs)^[10] and Az (with Cu(II) in the heme group).^[18] On the other hand, most apo-protein junctions including apo-Az,^[18] apo-AfFtn-AA^[10] and apo-halorhodopsin,^[16] are dominated by temperature-dependent CT with lower tunneling rates (or current) with respect to their counterparts with cofactors.^[14–16,19] So far it is still not completely clear why CT across junctions of holo-proteins is more efficient than CT along their apo counterparts. Likely, the cofactor can provide additional tunneling pathways,^[1,3,5,10,15,18] but potential changes due to the supramolecular structure (or quaternary structure of the protein) of the junctions cannot be excluded. This work establishes the importance of the supramolecular protein structure in the junctions and how it affects the measured currents.

The mechanism of CT depends on d . For small values of d , coherent tunneling dominates (with large values of β) while the CT mechanism changes to incoherent tunneling for large d (with small values of β).^[20,21] This switch in the mechanism of CT as a function of d has been observed for junctions with various types of molecular wires with $d = 3–4$ nm.^[20,22] For example, Frisbie et al.^[20] reported coherent tunneling with $\beta = 3.0$ nm⁻¹ for junctions with oligophenyleneimine wires with $d < 4$ nm, but incoherent hopping with $\beta = 0.9$ nm⁻¹ for $d > 4$ nm. Intermediate regimes have also been observed where the value $\beta = 0.28–2.0$ nm⁻¹ is low, yet the mechanism of CT is activationless.^[3,18] Han et al.^[22] reported three CT regimes for junctions with bis-thienylbenzene, where CT was activationless with $\beta = 2.9$ nm⁻¹ for small $d < 8$ nm, and with a low $\beta = 0.8$ nm⁻¹ and low E_a for $d = 8–16$ nm, but the CT mechanism was thermally activated with $\beta = 0.015$ nm⁻¹ for $d > 16$ nm. In junctions with AfFtn-AA, the effective value of d can be controlled by changing the Fe-ion loading from 500Fe, where the ferritins are flattened with a diameter of 3.9 nm, to 4500Fe loading where AfFtn-AA retains its globular shape with a diameter of 11.0 nm inside the junctions. Here, a transition from an activationless CT regime with large $\beta = 1.30 \pm 0.02$ nm⁻¹ to another activationless regime with a low $\beta = 0.28 \pm 0.01$ nm⁻¹ occurred at $d = 7.5$ nm.^[10] In contrast, thermally activated CT was observed across the junctions of apo-AfFtn-AA.^[10]

This work focuses on the role of structural order in biomolecular tunnel junctions of three different types of globular iron-storing proteins with cage-like structures (Figure 1). We specifically chose these proteins due to their highly symmetrical nature to avoid variations in CT rates induced by differences in protein orientations with respect to the surface normal as would be the case in asymmetrical proteins. Dps is responsible for protecting cells against oxidative stress and may sequester Fe(II) and/or may bind with DNA to prevent oxidative damage to it. Dps proteins store iron oxide with a capacity of up to 500 Fe ions per cage. The Dps protein used in this study was of *Listeria innocua* (Figure 1A) modified to increase the affinity to nanocarbon materials.^[23] The modification 12-amino acids modification at the N-terminus of each subunit protrude from

S. Lim
Institute for Digital Molecular Analytics and Science
Nanyang Technological University
59 Nanyang Drive, Experimental Medicine Building
Singapore 636921, Singapore

C. A. Nijhuis
Department of Molecules and Materials
MESA+ Institute for Nanotechnology, and Center for Brain-Inspired
Nano Systems (BRAINS)
Faculty of Science and Technology
University of Twente
P.O. Box 217, Enschede 7500 AE, The Netherlands
E-mail: c.a.nijhuis@utwente.nl

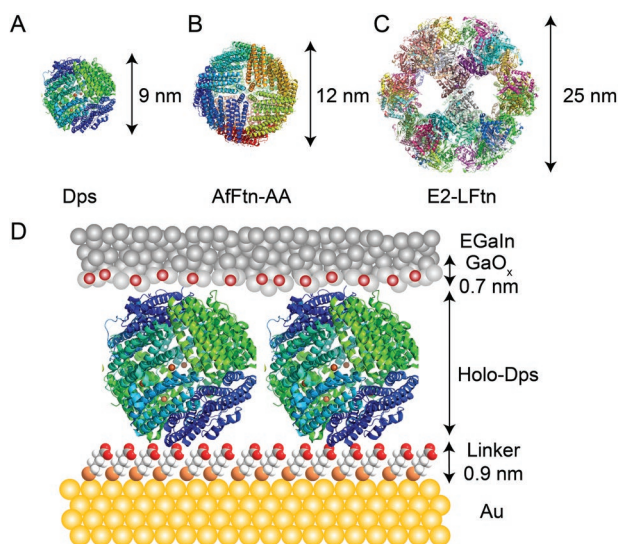


Figure 1. PyMOL rendition of A) Dps, B) AfFtn-AA, and C) E2-LFtn drawn to their relative scales; the double arrows indicate the respective diameters. D) A schematic representation of the Au-linker-holo-Dps//GaO_x/EGaIn junction, here “//” represents a van der Waal's contact and “/” represents the contact between GaO_x and the bulk eutectic metal.

the globular structure. This modification does not influence the experimental results in this work. It is stable up to 70 °C and consist of 12 identical subunits that self-assemble into a globular architecture with an outer diameter of 9 nm with a hollow cavity of 5 nm.^[24] The iron oxide NPs in Dps likely resembles that of ferritin due to the existence of only minor differences in the structures of Dps and ferritin.^[25] The ferritin used in this study is a modified form of ferritin derived from the hyperthermophilic archaeon *Archaeoglobus fulgidus*. The modification of two amino acids (K150 and R151) to alanines results in the closed-pore structure AfFtn-AA.^[26] It consists of 24 identical subunits that self-assemble to form a symmetrical structure with an external diameter of 12 nm with an 8 nm wide cavity, in the presence of a trace amount of divalent metals or ionic concentration of more than 250 mM (Figure 1B). In the absence of iron or divalent metals in solution, the majority of AfFtn-AA are in the dimeric (2 subunits) form. Adsorption on surfaces may favor the assembled globular form since it is expected that a large cage will bind stronger to a surface than a small dimer. This ferritin is thermostable with a denaturation temperature of ≈80 °C and stores up to ≈5000 Fe ions per cage in the form of ferrihydrite NPs. The properties are similar to other reported ferritins.^[27–29] Figure 1C shows an E2 protein of globular shape with a diameter of 25 nm^[11] and a 12 nm wide cavity. The E2 protein used in this study was derived from the pyruvate dehydrogenase multienzyme complex from an extremophile *Geobacillus stearothermophilus*^[30] and bioengineered with Fe binding peptides from frog M-mimicking ferritin to from E2-LFtn.^[11] The modified E2-LFtn stores Fe ions in the form of iron oxide NPs with a maximum of 3000 Fe ions per cage. Depending on the Fe-loading, AfFtn-AA and E2-LFtn flatten upon adsorption on Au surface with varying degree. The flattening on the Au surface (pancake-like structures) result from low Fe loadings but at high loadings, both AfFtn and E2-LFtn retain their

globular structures.^[10] In contrast, their apo analogues lack the structural integrity induced by the iron oxide NPs and form disordered layers of varying degrees with apo-Dps being the most rigid and E2-LFtn the least. The varied sizes and structural integrities make these proteins an ideal platform to study the role of structural order or rigidity in CT in conjunction with the cofactor. The study gives us new insights into the factors that determine the mechanism of CT across biomolecular junctions.

2. Results and Discussion

2.1. Description of the Junctions

Figure 1A–C shows the three proteins rendered with PyMOL and Figure 1D shows a schematic representation of an Au-linker-Dps//GaO_x/EGaIn (EgaIn is the liquid metal top-electrode which is the eutectic alloy of Ga and In metals in 3:1 ratio by weight that is widely used to form electrical contacts to monolayers).^[31] All the experimental methods, including junction fabrication, preparation of the protein solutions, and monolayer formation, used in this work are described in the Supporting Information. We prepared the Dps proteins^[23] (PDB ID 2BJY) and loaded them with Fe-ions with established methods which are described in Sections S1 and S2 (Supporting Information). The Fe-ion content of the Dps in this study was ≈510 Fe ions per cage as estimated from transmission electron microscopy (TEM). The corresponding TEM images are included in Section S2 (Supporting Information). The preparation of AfFtn-AA and E2-LFtn in solution and loading with iron, and their surface immobilization and characterization, have been reported before.^[1,10] In this work, we used similar methods to form the Dps monolayers which are briefly discussed here (see also Section S4, Supporting Information). The proteins were immobilized on the Au electrode with a “linker” monolayer derived from HS(CH₂)₅COOH and the carboxylic acid groups were activated with 1-ethyl-3-(3-dimethylaminopropyl) carbodiimide. These activated carboxylic acid groups then react with the amines at the periphery of the proteins to form amide bonds firmly anchoring the proteins to the Au electrode (Section S3, Supporting Information).^[10] The ultra-smooth Au electrodes were obtained by the standard template-stripping method as previously reported (Section S4, Supporting Information).^[32] The Dps monolayers were characterized with atomic force microscopy (AFM; Section S5, Supporting Information) and X-ray absorption spectroscopy (Section S6, Supporting Information).

2.2. Characterization of the Dps Monolayers

We characterized the Dps monolayers with tapping-mode AFM (Section S5, Supporting Information). **Figure 2A** shows an AFM image of a bare Au surface with a root-mean-square (rms) surface roughness of 0.45 nm over an area of 1 × 1 μm², which is similar to previously reported values for template-stripped Au surfaces.^[33] **Figure 2B** shows that holo-Dps readily forms a dense monolayer with a rms roughness of 1.44 nm over a 1 × 1 μm² area. The corresponding rms surface roughness of

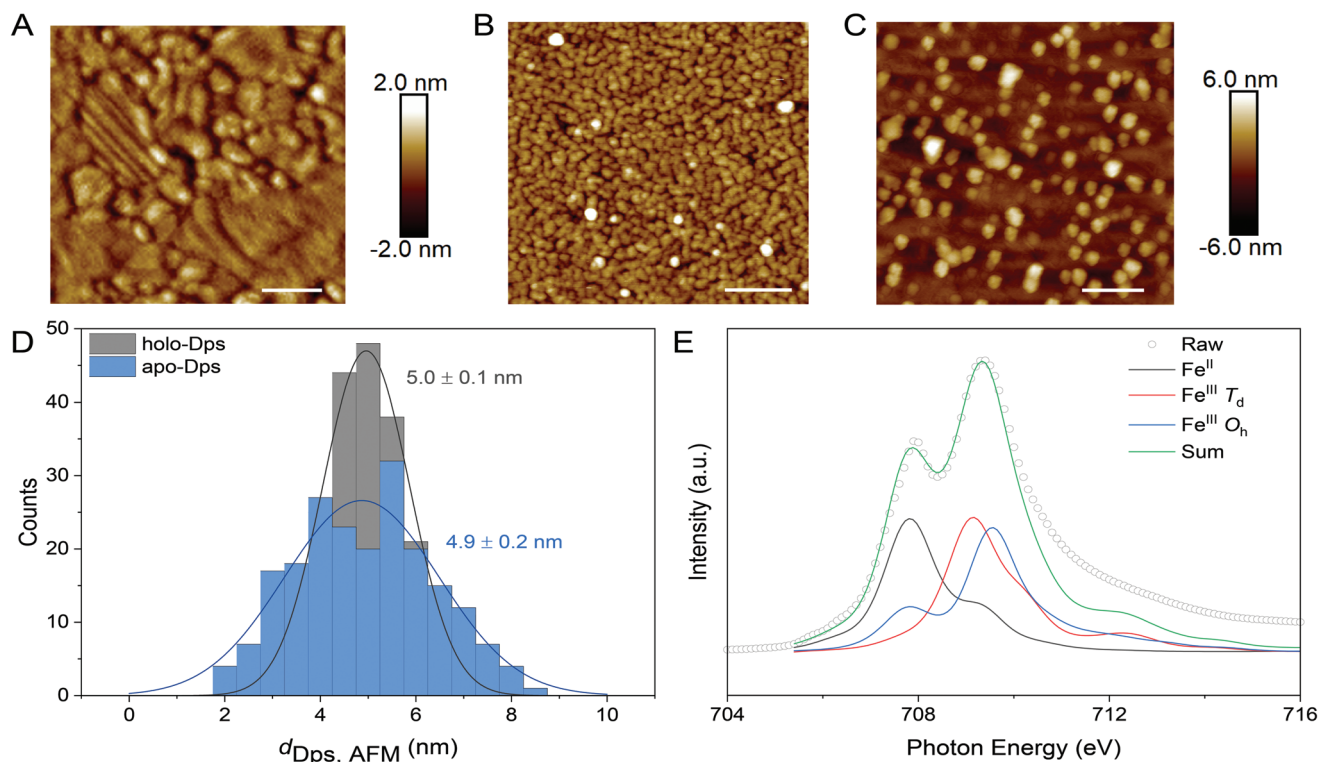


Figure 2. AFM images of A) a bare template-stripped Au substrate (scale bar: 200 nm), B) a dense holo-Dps monolayer (scale bar: 200 nm), and C) a holo-Dps submonolayer (scale bar: 100 nm). D) Histograms of the holo- and apo-Dps height distributions ($d_{Dps,AFM}$) obtained from the height profiles; solid lines represent Gaussian fits to these histograms. E) XAS spectrum of a Dps monolayer recorded at Fe $L_{3,2}$. The solid lines represent fits to the simulated spectra of Fe^{II} and Fe^{III} in O_h and T_d states.

the dense AfFtn-AA^[34] and E2-LFtn^[1] monolayers with maximum Fe-ion loadings of 4800Fe and 3000Fe, respectively, are 2.0 and 2.8 nm. The rms surface roughness increases with protein size as expected considering the globular nature of these proteins. To determine the height of immobilized Dps, we diluted the monolayer by reducing the adsorption time to 30 s allowing us to record AFM images of individual protein. Figure 2C shows an AFM image of a submonolayer where individual holo-Dps protein can be seen. We used a similar procedure^[1,10] to determine the Gaussian average height of Dps from the AFM height profiles, $d_{Dps,AFM}$, of both holo-Dps and apo-Dps of 5.0 ± 0.1 nm and 4.9 ± 0.2 nm, respectively (Figure S2, Supporting Information). The comparable size suggests that apo-Dps does not denature or flatten more on the surface than holo-Dps. The value of $d_{Dps,AFM}$ is significantly lower than the 9 nm diameter determined by crystallographic

studies,^[9] $d_{Dps,crys}$, which suggests that the Dps proteins flatten to a certain extent upon immobilization regardless of the Fe-ion loading. We attribute the difference in $d_{Dps,AFM}$ and $d_{Dps,crys}$ to the loss of water molecules^[35,36] (since our AFM measurements were carried out in air) and possibly by AFM tip-induced protein compression. The ratio of $d_{Dps,AFM}/d_{Dps}$, for holo-Dps is larger than the ratio for 500Fe AfFtn-AA or the ratio for 500Fe E2-LFtn (Table 1), which suggests that holo-Dps is less dynamic and flexible than AfFtn-AA and E2-LFtn with a similar Fe ion loading. A similar observation is made for the corresponding apo-proteins (Table 1). Based on these results, we conclude that Dps retains its spherical structure better on the surface than ferritin AfFtn-AA and E2-LFtn. We note that the Dps protein has a smaller cavity diameter (4.5 nm) than AfFtn-AA (8 nm) and E2-LFtn (12 nm) which likely explains the different degree of flattening.

Table 1. Summary of the d_{AFM} , d_{crys} and the ratio of d_{AFM}/d_{crys} .

a)	500Fe Dps	Apo-Dps	Apo-AfFtn-AA	500Fe AfFtn-AA	Apo-E2-LFtn	500Fe E2-LFtn
$d_{AFM}^{d)}$ [nm]	5.0 ± 0.1	4.9 ± 0.2	$3.6 \pm 0.2^{b)}$	$4.6 \pm 0.2^{b)}$	$6.9^{c)} \pm 0.3$	$11.0^{c)} \pm 0.3$
$d_{crys}^{e)}$ [nm]	9.0 ^{f)}	9.0 ^{f)}	12.0 ^{g)}	12.0 ^{g)}	24.0 ^{h)}	24.0 ^{h)}
d_{AFM}/d_{crys}	0.56	0.54	0.30	0.33	0.29	0.46

a) The numbers in parentheses indicate the iron ions per cage of the respective holo-proteins; b) Taken from ref. [10]; c) Taken from ref. [1]; d) Height profile from AFM experiments; e) Protein diameter from crystallographic studies; f) Taken from ref. [9]; g) Taken from ref. [37]; h) Taken from ref. [11].

2.3. Characterization of the Iron Oxide NPs in Holo-Dps

For the sake of completion, we characterized the composition of the holo-Dps immobilized on Au with X-ray absorption spectroscopy (XAS) at the Fe $L_{3,2}$ edge to resolve the ratio of Fe(II) and Fe(III) ions and their respective symmetry states (Section S6, Supporting Information). Figure 2E shows the XAS spectrum and the peak at 707.5 eV is attributed to Fe(II) and the peak at ≈ 709.2 eV is assigned to Fe^{III} in both octahedral (O_h) and tetrahedral (T_d) symmetries. The ratio of Fe(II) to Fe(III) ($R_1 = \text{Fe(II)}/\text{Fe(III)}$) was obtained by modeling the data with CTM4XAS software^[38] and the modeling parameters were taken from literature^[39] (see Section S6, Table S1, Supporting Information). The value of $R_1 = 0.63$ for Dps indicates that the iron oxide NPs in the holo-Dps is dominated by Fe(III), which is similar to other ferritins^[40,41] and the Afftn-AA reported by us.^[42] Unfortunately, in the case of E2-LFtn with 500Fe, the signal is too small in our XAS experiments likely because the NPs are encapsulated by a 12 nm thick protein shell and low surface concentration owing to the large size of the protein. We have reported the spectra for higher loadings, but the iron oxide NPs present in E2-LFtn is dominated by Fe(II) rather than Fe(III).^[1] These observations suggest that iron oxide in the Dps and Afftn-AA cores have similar compositions, despite some differences in structure and the ferroxidase center. In contrast, the structure of the iron oxide in the E2-LFtn core is distinct from the Dps and Afftn-AA.

2.4. Comparison of CT Rates and the Mechanism of CT across Fe-Binding Proteins

We followed previously reported procedures for the formation of the junctions with GaO_x/EGaIn top electrode stabilized in a through-hole connected to a microfluidic network in polydimethylsiloxane (PDMS), and the collection and analysis of the current-voltage, $J(V)$, data (Section S7, Supporting Information).^[43] We recorded 347 and 339 $J(V)$ traces from junctions with monolayers of both holo- and apo-Dps, respectively, and plotted the $\log_{10}|J|$ at each V in histograms that were fitted to a Gaussian function to obtain the Gaussian average, $\langle \log_{10}|J| \rangle_G$, and the log standard deviation, σ_{\log} , of the current density (Section S8, Supporting Information). **Figure 3A** shows the $\langle \log_{10}|J| \rangle_G$ plotted against the voltage for junctions with apo-proteins, and **Figure 3B** shows that of junctions with holo-proteins. The $J(V)$ characteristics of the junctions with Afftn-AA^[10] (also measured with EGaIn stabilized in a through-hole in PDMS^[43]) and E2-LFtn^[1] (measured with cone-shaped tips of EGaIn^[44]) have been reported; the corresponding results are presented in **Figure 3A,B** (all with 500 Fe loading) to compare the behavior of these junctions across the three different types of proteins. The J is an extensive parameter since it depends on the effective electrical contact area A_{eff} (which may be orders of magnitude smaller than the geometrical contact area A_{geo}) of the junction. The effective contact area in junctions with cone-shaped tips, however, is similar to junctions with the EGaIn stabilized in a through-hole.^[43,45] Therefore, the results in **Figures 3A-B** can be directly compared. The conductivity of the junctions with holo-Dps is 2 times larger than

those junctions with apo-Dps. This observation is attributed to the presence of the iron oxide NPs which provides accessible energy states increasing the tunneling rates. We also note that the presence of Fe-ions enhances the mechanical stability of the protein^[1,36] and improves structural order which may assist with CT by facilitating efficient intrachain pathways. This result agrees with those from other studies where it has been reported that the presence of metal oxide cores or cofactors increase the CT rates, e.g., junctions with Az,^[14] halorhodopsin,^[16] E2-LFtn^[1] and cytochrome-C.^[15] Interestingly, the values of J across the junctions with the proteins in this study are remarkably similar, i.e., J across junctions with Dps (J_{Dps}) of E2-LFtn ($J_{\text{E2-LFtn}}$) is comparable to J across the junctions of E2-LFtn ($J_{\text{E2-LFtn}}$) or Afftn-AA ($J_{\text{Afftn-AA}}$). This counter-intuitive order of $J_{\text{E2-LFtn}} \approx J_{\text{Afftn-AA}} \approx J_{\text{Dps}}$ (which holds for holo- and apo-proteins) is surprising as E2-LFtn forms much thicker monolayers (11 nm) than Dps (4.6 nm; Table 1). More specifically, in the case of both coherent and incoherent tunneling, the value of J decreases with increasing monolayer thickness and should in principle follow the order $J_{\text{Dps}} > J_{\text{Afftn-AA}} > J_{\text{E2-LFtn}}$. The different types of proteins may respond differently to the pressure applied by the top-electrode resulting in varying degrees of the reduction of the tunneling distance defined by the monolayer. Following this line of thought, our results suggest that the deformation (or flattening) of the proteins induced by the EGaIn top-electrode increases with protein size and is thus the largest for E2-LFtn. It is to keep in mind that the mechanism of CT may differ which could also explain the surprising trend in current densities. Therefore, we carried out $J(V)$ measurements as a function of temperature to elucidate the CT mechanism.

2.5. The Mechanisms of Charge Transport

To conduct $J(V, T)$ measurements, we formed Dps monolayers on a patterned array of Au bottom electrodes (the Au electrodes were fabricated using reported procedures^[46]). We contacted the monolayers with GaO_x/EGaIn stabilized in PDMS microchannels which were aligned perpendicularly over the Au electrodes. The fabrication and experimental procedures for $J(V, T)$ measurements are described in detail in Sections S9 and S10 (Supporting Information). We restricted the maximum T in our investigation to 320 K as Dps proteins reportedly start to melt around $T = 320$ K.^[47] **Figure 3C** shows the $J(V, T)$ data obtained from a junction with a monolayer of apo-Dps for $T = 230$ –320 K and **Figure 3D** shows the same but for a junction with holo-Dps for $T = 175$ –320 K (additional data sets are given in Section S10, Supporting Information). The corresponding Arrhenius plots (**Figure 3E–F**) plotted at $V = -0.5$ V show that the mechanism of CT across the apo-Dps and holo-Dps junctions is activationless indicating that the mechanism of CT is coherent tunneling. Although activationless CT across holo-proteins has been reported before,^[10,15–19] to the best of our knowledge, this is the first time that activationless CT across an apo-protein junction is found. We note that apo-Dps retains its globular geometry better than apo-E2-LFtn and apo-Afftn-AA, as discussed above (Table 1). Therefore, we suggest that CT across apo-Dps can readily proceed along organized protein segments and the CT rate is limited by intrachain tunneling

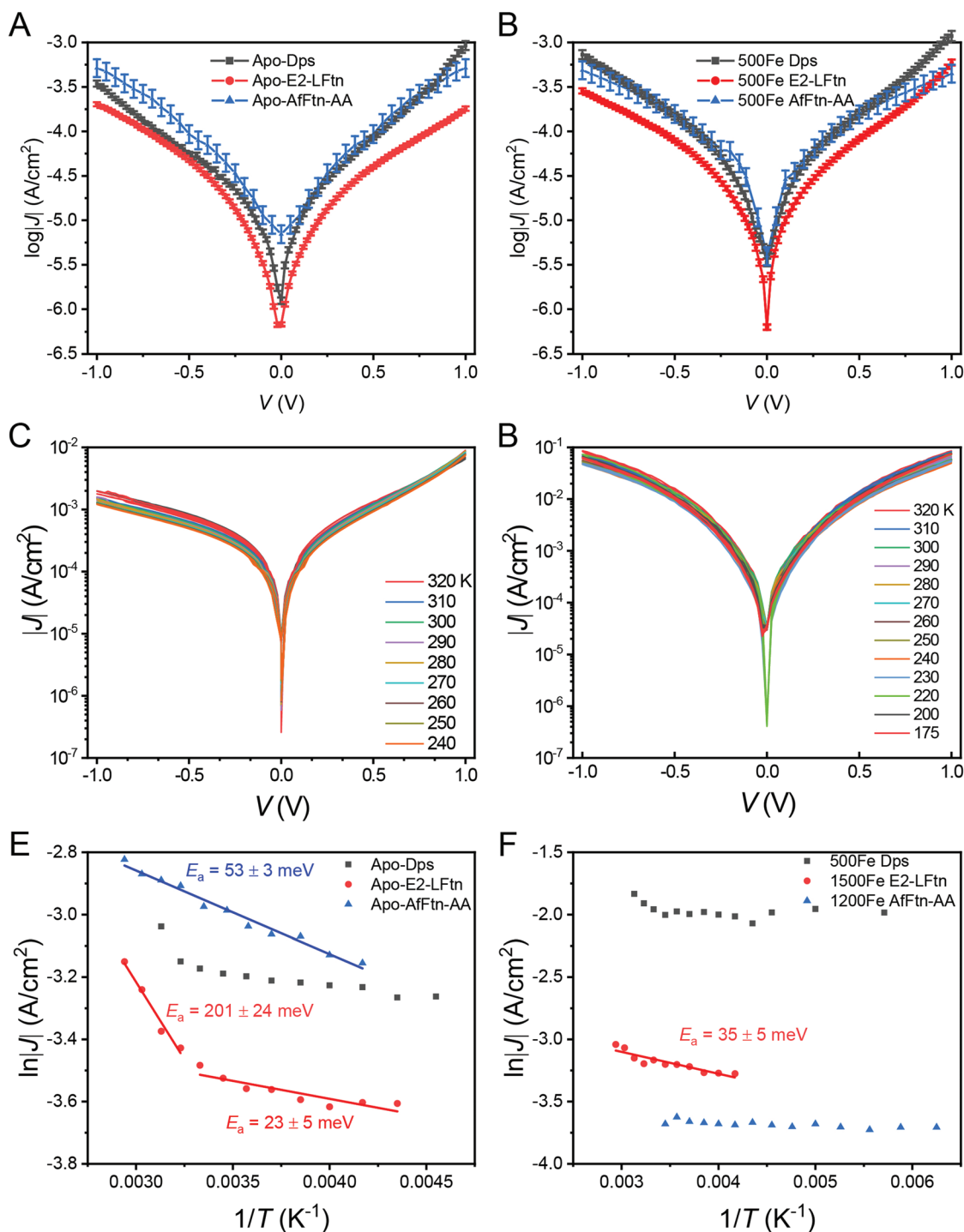


Figure 3. The $\langle \log_{10}|J| \rangle_C$ versus V curves of Dps, AfFtn-AA (data taken from ref. [10]), and E2-LFtn (data taken from ref. [1]) recorded from junctions with A) apo-proteins and B) holo-proteins, all with 500 Fe loading. The error bars represent the 95% confidence bands. The raw $J(V, T)$ data for C) apo-Dps and D) holo-Dps and the corresponding Arrhenius plots at $V = -0.5$ V, in comparison of J for apo-proteins E) and holo-proteins F) with lowest Fe ion loadings.

steps with small, if at all, energy barriers (to observe low energy barriers, CT studies at much lower T would be needed which are not feasible as unfortunately, the junctions shorted at $T < 150$ K likely due to cold denaturation of Dps). In a previous report, we suggested that in the absence of an organized

CT pathway, CT proceeds via incoherent tunneling where charges have to hop between different, disordered protein segments.^[1] This hypothesis explains why CT across apo-E2-LFtn and apo-AfFtn-AA junctions is thermally activated as these proteins form dense, disordered monolayers where charges are

forced to hop across disordered protein segments separated by relatively large energy barriers.

To address the question why apo-E2-LFtn is the most conductive protein, we also plotted the previously reported Arrhenius plots obtained from junctions with AfFtn-AA (taken from ref. [10]) and E2-LFtn (taken from ref. [1]) in Figures 3E,F. It is important to note that E_a is an intensive parameter that is independent of the junction area and, consequently, it can be directly compared across the different types of EGaIn junctions. In principle, the J in the Arrhenius plots in Figures 3E-F for the three different proteins (which were all obtained with different variations of the “EGaIn-technique”), can be corrected with a correction factor A_f for the effective electrical contact area, $A_f = A_{\text{eff}}/A_{\text{geo}}$, by accounting for the differences in surface roughness of the electrodes as detailed in previous work. However, in the current study the large proteins (e.g., E2-LFtn) themselves also modify the surface topography of the electrodes and they may respond differently to the pressure applied by the top electrode on the monolayer and therefore we refrain ourselves from correcting the J in Figure 3E-F for A_f and we focus the discussion solely on E_a values.

The mechanism of CT across apo-E2-LFtn junctions is incoherent tunneling with a large $E_a = 254 \pm 34$ meV for $T = 340\text{--}300$ K, while AfFtn-AA junctions have a lower $E_a = 58 \pm 7$ meV for $T = 340\text{--}240$ K. Completely incoherent tunneling is only weakly dependent on $d^{[4]}$ and, consequently, the differences in d are negated by this change in the mechanism of CT. Incoherent tunneling offers high CT rates at high T due to the availability of various high energy vibrational modes^[48] which dominate the current densities for junctions with apo-E2-LFtn. This incoherent tunneling component is likely to be smaller for apo-AfFtn-AA than that for E2-LFtn, and is negligible in apo-Dps, explaining why apo-E2-LFtn shows the highest conductance. Thus, in essence, we observe a relation between protein size after immobilization and the incoherent tunneling component of CT across tunnel junctions with the apo-proteins. It is interesting to note that the values of E_a follow the order of the $d_{\text{AFM}}/d_{\text{crys}}$ ratio (Table 1) which is a measure of structural order as explained earlier: the ratio is the highest for Dps where E_a is negligible, and the ratio is the smallest for E2-LFtn which has the highest value of E_a . These results suggest that the disorder in the protein monolayer is responsible for the differences in the mechanism of CT and the observed J . We would like to note that for junctions with apo-E2-LFtn, an incoherent tunneling regime is observed with a low $E_a = 23 \pm 5$ meV at low $T < 290$ K which likely represents intra-chain tunneling as at these low temperatures the energy required to overcome large energy barriers is not sufficient.^[1]

The behavior of the junctions with holo-proteins can be explained as follows. Figure 3F shows the Arrhenius plots of the junctions. The mechanism of CT is thermally activated with $E_a = 35 \pm 5$ meV the thickest junction (Table 1) with holo-E2-LFtn which is a substantial reduction of the $E_a = 254 \pm 34$ meV for the junctions with apo-E2-LFtn. In the case of the holo-AfFtn-AA, the thermally activated component is absent and the CT across holo-Dps is activationless. The metal oxide core provides alternative tunneling sites which explains the 2-fold increase in the tunneling rates in the case of the Dps junctions, and the removal of the thermally activated component in the AfFtn-AA

junctions. In contrast, CT across junctions of holo-E2-LFtn proceeds by incoherent tunneling, which can be explained by disorder in the protein monolayers: the new conduction channels introduced by the metal oxide core cannot compensate enough for structural disorder and the associated thermally activated component.

3. Conclusions

We investigated CT across Fe-storing Dps protein-based tunnel junctions. Our AFM data suggest that the Dps proteins are more rigid than AfFtn-AA and E2-LFtn. Dps retains the globular architecture upon immobilization on Au. In EGaIn junctions, the mechanism of CT is activationless for both apo-Dps and holo-Dps, which suggests that the CT proceeds by a coherent tunneling mechanism in both Dps proteins. Although coherent tunneling across ordered apo-proteins has been reported before, to the best of our knowledge, activationless CT suggesting coherent tunneling across an apo-protein has not been previously reported. Coherent tunneling across holo-Dps is expected because the presence of Fe ions increases the CT rates by providing alternative energy states for coherent tunneling. We suggest that the retention of the globular architecture in apo-Dps provides efficient conduction pathways that allow for activationless CT across the protein backbone. This hypothesis is reinforced by comparing temperature dependent $J(V)$ data obtained from junctions with apo-AfFtn-AA and apo-E2-LFtn which suffer progressively from more disorder. Our study reveals that the mechanism of the CT across these biomolecular junctions strongly relates to the degree to which a protein immobilized on an electrode retains its natural quaternary structure. The presence of the metal oxide cores or cofactors, besides providing alternative electronic states for tunneling, also plays an important role in the stabilization of the quaternary structure of proteins. Our results provide insights to improve the understanding of CT across biological systems.

Supporting Information

Supporting Information is available from the Wiley Online Library or from the author.

Acknowledgements

N.K.G. and N.O. contributed equally to this work. The authors acknowledge the Soft X-ray Spectroscopy beamline at the Australian Synchrotron, part of ANSTO, for their help with the XAS characterization, and Dr. Anton Tadich for assistance with the experimentation. Prime Minister's Office, Singapore, is acknowledged for supporting this research under its Medium-sized Centre Program. A portion of this work was also supported by JST CREST Grant Number JPMJCR1813, Japan.

Conflict of Interest

The authors declare no conflict of interest.

Data Availability Statement

The data that support the findings of this study are available from the corresponding author upon reasonable request.

Keywords

biomolecular electronics, charge transport, EGaIn, structural order, tunneling

Received: May 30, 2022

Revised: July 19, 2022

Published online: September 14, 2022

- [1] N. K. Gupta, R. R. Pasula, S. K. Karuppannan, Z. Ziyu, A. Tadich, B. Cowie, D.-C. Qi, P. Bencok, S. Lim, C. A. Nijhuis, *J. Mater. Chem. C* **2021**, 9, 10768.
- [2] K. Garg, M. Ghosh, T. Eliash, J. H. Van Wonderen, J. N. Butt, L. Shi, X. Jiang, F. Zdenek, J. Blumberger, I. Pecht, M. Sheves, D. Cahen, *Chem. Sci.* **2018**, 9, 7304.
- [3] N. Amdursky, D. Marchak, L. Sepunaru, I. Pecht, M. Sheves, D. Cahen, *Adv. Mater.* **2014**, 26, 7142.
- [4] C. D. Bostick, S. Mukhopadhyay, I. Pecht, M. Sheves, D. Cahen, D. Lederman, *Rep. Prog. Phys.* **2018**, 81, 026601.
- [5] J. Blumberger, *Chem. Rev.* **2015**, 115, 11191.
- [6] D. N. Beratan, *Annu. Rev. Phys. Chem.* **2019**, 70, 71.
- [7] K. Michaeli, D. N. Beratan, D. H. Waldeck, R. Naaman, *Proc. Natl. Acad. Sci. USA* **2019**, 116, 5931.
- [8] N. L. Ing, M. Y. El-Naggar, A. I. Hochbaum, *J. Phys. Chem. B* **2018**, 122, 10403.
- [9] R. A. Grant, D. J. Filman, S. E. Finkel, R. Kolter, J. M. Hogle, *Nat. Struct. Biol.* **1998**, 5, 294.
- [10] S. K. Karuppannan, R. R. Pasula, S. Lim, C. A. Nijhuis, *Adv. Mater.* **2016**, 28, 1824.
- [11] T. Peng, D. Paramelle, B. Sana, C. F. Lee, S. Lim, *Small* **2014**, 10, 3131.
- [12] D. Xu, G. D. Watt, J. N. Harb, R. C. Davis, *Nano Lett.* **2005**, 5, 571.
- [13] D. N. Axford, J. J. Davis, *Nanotechnology* **2007**, 18, 145502.
- [14] I. Ron, L. Sepunaru, S. Itzhakov, T. Belenkova, N. Friedman, I. Pecht, M. Sheves, D. Cahen, *J. Am. Chem. Soc.* **2010**, 132, 4131.
- [15] N. Amdursky, I. Pecht, M. Sheves, D. Cahen, *J. Am. Chem. Soc.* **2013**, 135, 6300.
- [16] S. Mukhopadhyay, S. Dutta, I. Pecht, M. Sheves, D. Cahen, *J. Am. Chem. Soc.* **2015**, 137, 11226.
- [17] L. Sepunaru, N. Friedman, I. Pecht, M. Sheves, D. Cahen, *J. Am. Chem. Soc.* **2012**, 134, 4169.
- [18] L. Sepunaru, I. Pecht, M. Sheves, D. Cahen, *J. Am. Chem. Soc.* **2011**, 133, 2421.
- [19] S. Raichlin, I. Pecht, M. Sheves, D. Cahen, *Angew. Chem, Int. Ed.* **2015**, 54, 12379.
- [20] S. Ho Choi, B. Kim, C. D. Frisbie, *Science* **2008**, 320, 1482.
- [21] C. Joachim, M. A. Ratner, *Proc. Natl. Acad. Sci. USA* **2005**, 102, 8801.
- [22] H. Yan, A. J. Bergren, R. McCreery, M. L. Della Rocca, P. Martin, P. Lafarge, J. C. Lacroix, *Proc. Natl. Acad. Sci. USA* **2013**, 110, 5326.
- [23] M. Ito, N. Okamoto, R. Abe, H. Kojima, R. Matsubara, I. Yamashita, M. Nakamura, *Appl. Phys. Express* **2014**, 7, 065102.
- [24] T. Haikarainen, A. C. Papageorgiou, *Cell. Mol. Life Sci.* **2010**, 67, 341.
- [25] M. Su, S. Cavallo, S. Stefanini, E. Chiancone, N. D. Chasteen, *Biochemistry* **2005**, 44, 5572.
- [26] B. Sana, E. Johnson, P. Le Magueres, A. Criswell, D. Cascio, S. Lim, *J. Biol. Chem.* **2013**, 288, 32663.
- [27] N. D. Chasteen, P. M. Harrison, *J. Struct. Biol.* **1999**, 126, 182.
- [28] N. Jian, M. Dowle, R. D. Horniblow, C. Tselepis, R. E. Palmer, *Nanotechnology* **2016**, 27, 46LT02.
- [29] X. Liu, W. Jin, E. C. Theil, *Proc. Natl. Acad. Sci. USA* **2003**, 100, 3653.
- [30] M. Dalmau, S. Lim, H. C. Chen, C. Ruiz, S.-W. Wang, *Biotechnol. Bioeng.* **2008**, 101, 654.
- [31] D. Thompson, C. A. Nijhuis, *Acc. Chem. Res.* **2016**, 49, 2061.
- [32] E. A. Weiss, G. K. Kaufman, J. K. Kriebel, Z. Li, R. Schalek, G. M. Whitesides, *Langmuir* **2007**, 23, 9686.
- [33] L. Yuan, L. Jiang, D. Thompson, C. A. Nijhuis, *J. Am. Chem. Soc.* **2014**, 136, 6554.
- [34] S. Mukhopadhyay, S. K. Karuppannan, C. Guo, J. A. Fereiro, A. Bergren, V. Mukundan, X. Qiu, O. E. Castañeda Ocampo, X. Chen, R. C. Chiechi, R. McCreery, I. Pecht, M. Sheves, R. R. Pasula, S. Lim, C. A. Nijhuis, A. Vilan, D. Cahen, *iScience* **2020**, 23, 101099.
- [35] J. Zhang, C. Cui, X. Zhou, *Chin. Sci. Bull.* **2009**, 54, 723.
- [36] T. Rakshit, S. Banerjee, S. Mishra, R. Mukhopadhyay, *Langmuir* **2013**, 29, 12511.
- [37] M. Uchida, S. Kang, C. Reichhardt, K. Harlen, T. Douglas, *Biochim. Biophys. Acta, Gen. Subj.* **2010**, 1800, 834.
- [38] E. Stavitski, F. M. F. de Groot, *Micron* **2010**, 41, 687.
- [39] P. Kuiper, B. Searle, L.-C. Duda, R. Wolf, P. van der Zaag, *J. Electron Spectrosc. Relat. Phenom.* **1997**, 86, 107.
- [40] M. Koralewski, L. Balejíčková, Z. Mitróová, M. Pochylski, M. Baranowski, P. Kopčanský, *ACS Appl. Mater. Interfaces* **2018**, 10, 7777.
- [41] Y. H. Pan, K. Sader, J. J. Powell, A. Bleloch, M. Gass, J. Trinick, A. Warley, A. Li, R. Brydson, A. Brown, *J. Struct. Biol.* **2009**, 166, 22.
- [42] S. K. Karuppannan, R. R. Pasula, T. S. Herng, J. Ding, X. Chi, E. Del Barco, S. Roche, X. Yu, N. Yakovlev, S. Lim, C. A. Nijhuis, *J. Phys. Mater.* **2021**, 4, 035003.
- [43] A. Wan, L. Jiang, C. S. S. Sangeeth, C. A. Nijhuis, *Adv. Funct. Mater.* **2014**, 24, 4442.
- [44] N. Nerngchamnong, L. Yuan, D.-C. Qi, J. Li, D. Thompson, C. A. Nijhuis, *Nat. Nanotechnol.* **2013**, 8, 113.
- [45] S. K. Karuppannan, H. Hongting, C. Troadec, A. Vilan, C. A. Nijhuis, *Adv. Funct. Mater.* **2019**, 29, 1904452.
- [46] C. A. Nijhuis, W. F. Reus, J. R. Barber, M. D. Dickey, G. M. Whitesides, *Nano Lett.* **2010**, 10, 3611.
- [47] S. Franceschini, P. Ceci, F. Alaleona, E. Chiancone, A. Ilari, *FEBS J.* **2006**, 273, 4913.
- [48] M. Bixon, J. Jortner, *J. Am. Chem. Soc.* **2001**, 123, 12556.